



Gas Sensors Hot Paper

How to cite: *Angew. Chem. Int. Ed.* **2021**, *60*, 25758–25761

International Edition: doi.org/10.1002/anie.202111519

German Edition: doi.org/10.1002/ange.202111519

# Layer-by-Layer Growth of Preferred-Oriented MOF Thin Film on Nanowire Array for High-Performance Chemiresistive Sensing

Yuan Lin<sup>†</sup>, Wen-Hua Li<sup>†</sup>, Yingyi Wen, Guan-E Wang, Xiao-Liang Ye, and Gang Xu<sup>\*</sup>

**Abstract:** High-quality MOF thin films with high orientation and controlled thickness are extremely desired for applications. However, they have been only successfully fabricated on flat substrates. Those MOF 2D thin films are limited by low exposed area and slow mass transport. To overcome these issues, MOF 3D thin films with good crystallinity, preferred orientation, and precisely controllable thickness in nanoscale were successfully prepared in a controllable layer-by-layer manner on nanowire array substrate for the first time. The as-prepared Cu-HHTP 3D thin film is superior to corresponding 2D thin films and showed one of the highest sensitivity, lowest LOD, and fastest response among all reported chemiresistive NH<sub>3</sub> sensing materials at RT. This work provides a feasible approach to grow preferred-oriented 3D MOF thin film, offering new perspectives for constructing MOF-based heterostructures for advanced applications.

**M**etal–organic frameworks (MOFs) with well-designable structures, high surface area and highly exposed active sites, have become promising candidates in gas storage and separation, catalysis, sensors, etc.<sup>[1–8]</sup> To facilitate their application in advanced electrical devices, various thin film preparation methods have been explored on MOFs, such as layer-by-layer liquid phase epitaxy (LBL-LPE), Langmuir–Blodgett LBL deposition, and post assembly of MOF nanocrystals.<sup>[9–20]</sup> At present, on flat substrates (such as Au film/Si and quartz wafer), high-quality MOF thin films with high orientation and controlled thickness in nanoscale (denoted as oriented MOF 2D thin film, Scheme 1) have been successfully prepared.<sup>[21–23]</sup> However, many applications including catalysis, sensing, and electrochemical energy storage, require MOF thin films to be grown on 3D nanostructured substrates (e.g., porous substrates, nanowire array substrates).<sup>[24–26]</sup> Such

nanostructured MOF thin films (denote as oriented MOF 3D thin film, Scheme 1) gain not only higher surface area but also faster charge and mass transport, giving rise to better performances. Nevertheless, the controllable preparation of MOF 3D thin films remains a great challenge and the reported direct growth methods can not realize preferred orientation and controlled thickness.<sup>[27–29]</sup> Notably, LBL deposition provides not only oriented growth but also precise thickness control in nanoscale, which is an extremely desired approach for preparing MOF 3D thin films and optimizing performances.

In this work, LBL growth of 3D MOF thin film on nanowire array (NWA) substrate was reported for the first time. This was realized by repeatedly immersing TiO<sub>2</sub> nanowire array in the solution of Cu<sup>2+</sup> ion and that of 2, 3, 6, 7, 10, 11-hexahydroxytriphenylene (HHTP) ligand at 45 °C, respectively. The preferred orientation and controlled LBL growth process of Cu-HHTP 3D thin film were studied by transmission electron microscopy (TEM) and powder X-ray diffraction (PXRD). Compared with 2D thin film, Cu-HHTP 3D thin film offers much larger surface area and shorter charge and mass transport pathway. As an exemplary application, semiconducting Cu-HHTP 3D thin film was fabricated as room-temperature chemiresistive NH<sub>3</sub> gas sensor, which showed 2.5 times enhanced response (to 1 ppm NH<sub>3</sub>), more than 1000 times optimized limit of detection (LOD), and 2.3 times improved response speed than corresponding 2D thin film.

Cu-HHTP 3D thin films were prepared by a modified LBL-LPE approach (details see Supporting Information). Compared with reported LBL-LPE method for growing MOF 2D thin films, the modified preparation strategy has following features: 1) instead of flat substrates, nanowire array was used; 2) the reaction temperature was finely tuned from room temperature to 45 °C to optimize the nucleation/

[\*] Y. Lin,<sup>[†]</sup> Dr. W.-H. Li,<sup>[†]</sup> Y. Wen, Dr. G.-E. Wang, Dr. X.-L. Ye, Prof. G. Xu  
Fujian Science & Technology Innovation Laboratory for Optoelectronic Information of China  
Fuzhou, Fujian 350108 (P. R. China)  
E-mail: gxu@fjirsm.ac.cn

Y. Lin,<sup>[†]</sup> Y. Wen, Prof. G. Xu

State Key Laboratory of Structural Chemistry, Fujian Institute of Research on the Structure of Matter, Chinese Academy of Sciences (CAS)

No. 155 Yangqiao Road West, Fuzhou, Fujian 350002 (P. R. China) and

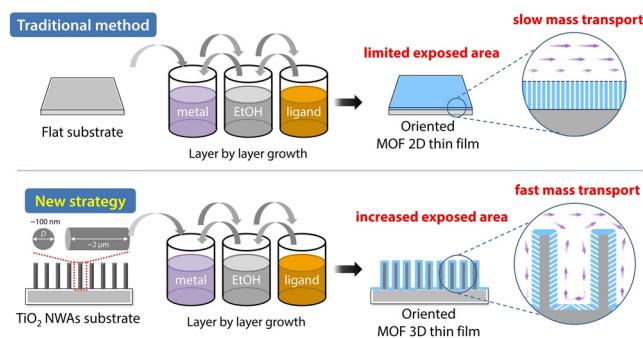
University of Chinese Academy of Sciences (UCAS)

No. 19A Yuquan Road, Beijing 100049 (P. R. China)

[†] These authors contributed equally to this work.

Supporting information and the ORCID identification number(s) for the author(s) of this article can be found under:

<https://doi.org/10.1002/anie.202111519>.



**Scheme 1.** Difference between MOF 2D thin film and MOF 3D thin film.

growth process and enhance crystallinity. Firstly, single-crystal  $\text{TiO}_2$  nanowires with a diameter of 50–100 nm and a length of  $\approx 2 \mu\text{m}$  were grown on sapphire substrate with a hydrothermal method (Figure S1). Secondly, the obtained  $\text{TiO}_2$  NWAs were immersed into  $\text{Cu}(\text{OAc})_2$  and HHTP solutions, respectively, to grow Cu-HHTP thin film in a LBL manner. Between each immersion process,  $\text{TiO}_2$  NWAs were washed by ethanol to remove unreacted reagent. The concentration of the reagent solutions, reaction temperature and immersion duration were tuned to optimize the quality of Cu-HHTP 3D thin film (see Supporting Information).

Figure S1, 1b and S2 show the cross-sectional and top-view SEM images of  $\text{TiO}_2$ -NWAs and Cu-HHTP 3D thin film with a thickness of 20 nm (denoted as Cu-HHTP-20 nm).  $\text{TiO}_2$  nanowires interlace with each other at the middle of the length, which was unchanged after thin-film growth. Cu-HHTP thin film on the interlaced  $\text{TiO}_2$  nanowires forms a continuous 3D nanostructure, which was detailedly studied by TEM. Figure 1c, S3 and S4 show a homogeneous Cu-HHTP thin film of 20 nm coating on a  $\text{TiO}_2$  nanowire to form a core-sheath nanostructure. A clear interface between  $\text{TiO}_2$  and Cu-HHTP could be observed by different contrast. The lattice fringes of MOF sheath showed a pitch of  $\approx 1.8 \text{ nm}$ , corresponding to the (100) facets of Cu-HHTP (Figure 1d). This demonstrates that the growth of Cu-HHTP film is along the [001] direction. Statistical analysis showed the angles between 1D channels of Cu-HHTP and  $\text{TiO}_2$  surface mainly range from 60 to 80° (Figure 1e). Element mapping by high-angle

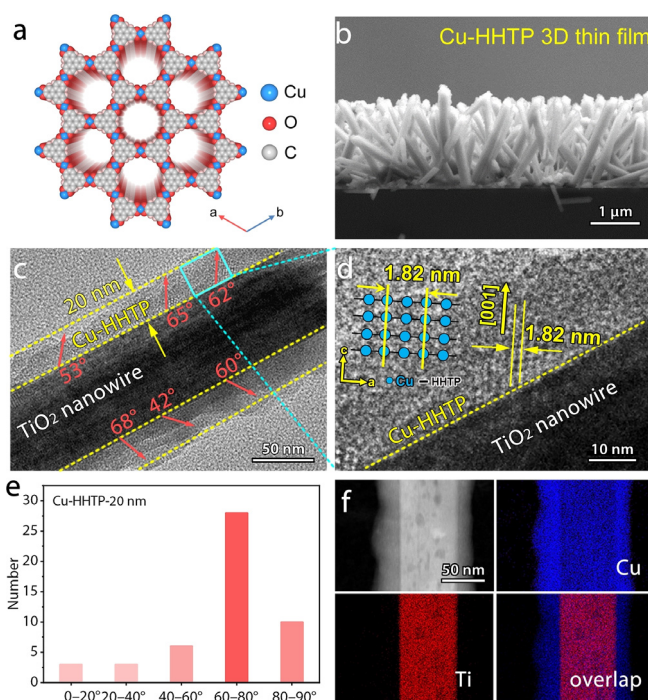


**Figure 1.** (a) Crystal structure of Cu-HHTP. (b) Scanning electron microscopy (SEM) image of Cu-HHTP 3D thin film grown on  $\text{TiO}_2$ -NWAs substrate. (c) FETEM image and (d) lattice fringes of Cu-HHTP thin film on a  $\text{TiO}_2$  nanowire. (e) Statistical analysis of the preferred-oriented angle of crystal domains in Cu-HHTP 3D thin film. (f) HAADF EDS elemental mapping.

annular dark field (HAADF) energy-dispersive X-ray spectroscopy (EDS) further confirmed this  $\text{TiO}_2/\text{Cu-HHTP}$  core-sheath structure (Figure 1f and S5), suggesting the preferred-oriented growth of the Cu-HHTP crystal domains. Notably, orientation is crucial for the exposure of pores and active sites in Cu-HHTP to facilitate applications.

It has been reported that Cu-HHTP 2D thin film can be epitaxially grown on a -OH group functionalized quartz plate by a LBL spray method.<sup>[25]</sup> In this work,  $\text{TiO}_2$  nanowires have a small amount of -OH groups ununiformly distributed on their surfaces (Figure S6, S7). At the initial stage of thin film growth, an island-type nucleation process rather than uniform epitaxy dominated (Figure 2a). In the following growth cycles, Cu-HHTP nano-islands extended slowly and then merged. A continuous thin film with a thickness of  $\approx 6 \text{ nm}$  could be obtained at the 8th cycle (Figure 2b). After that, the growth of Cu-HHTP thin film accelerated and the thickness increased linearly at a rate of  $\approx 2 \text{ nm}$  per cycle (Figure 2b–f). Figure 2b–e and S8 show typical 6, 12, 20 and 36 nm Cu-HHTP thin films obtained by 8, 12, 16 and 24 growing cycles, respectively.

The schematic diagram and the optical photograph of a Cu-HHTP 3D thin-film device were shown in Figure 3a.

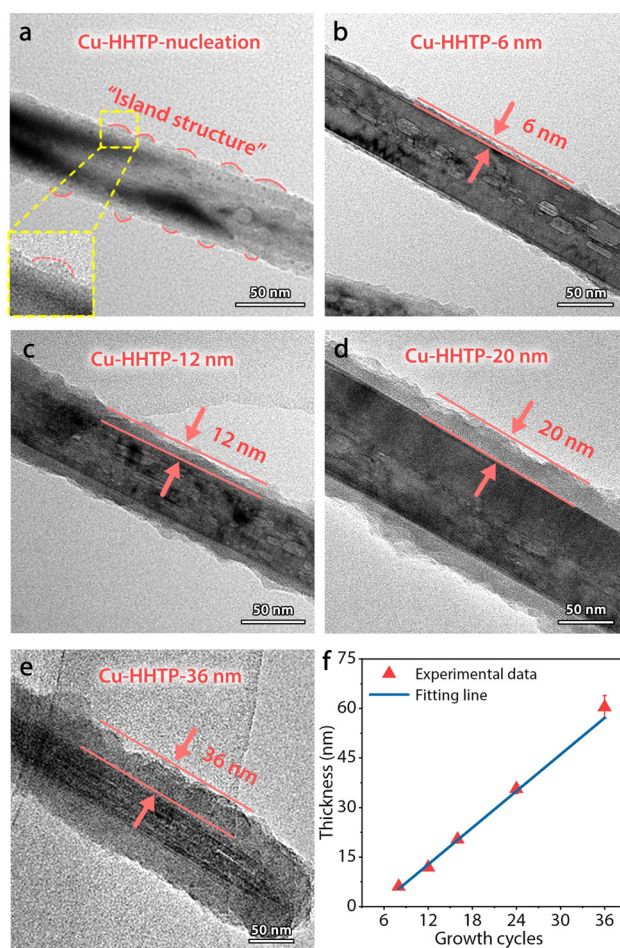


**Figure 2.** TEM images of Cu-HHTP 3D thin film: (a) nucleation layer, (b) 6 nm, (c) 12 nm, (d) 20 nm and (e) 36 nm, respectively. (f) Growth cycles-dependent thickness of Cu-HHTP 3D thin film.

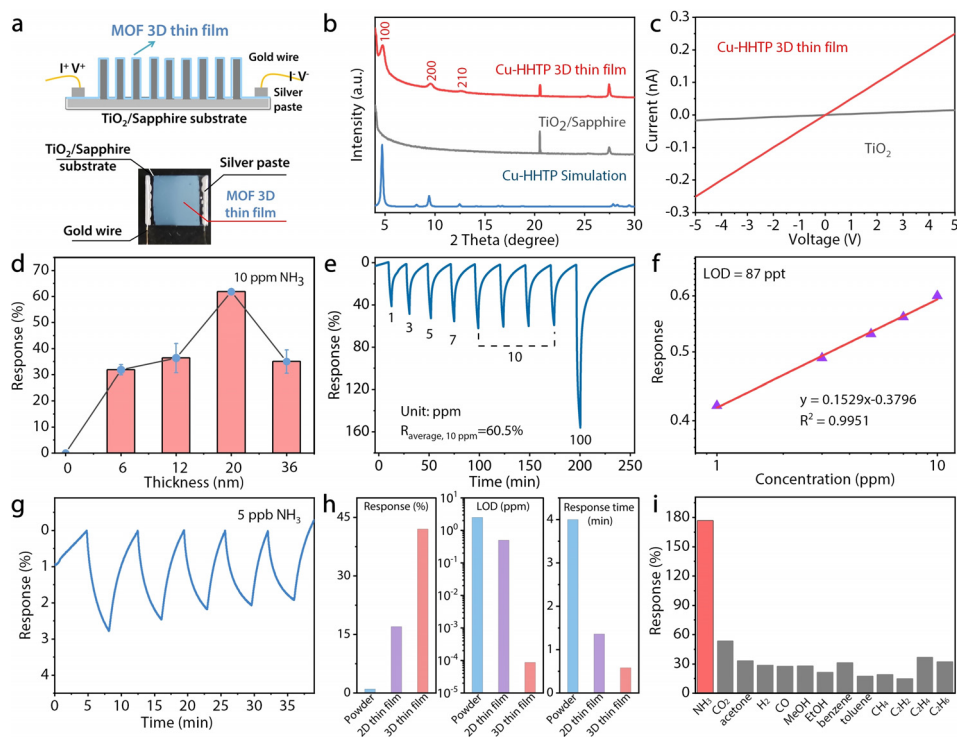


**Figure 3.** (a) Schematic drawing and optical photograph of a MOF 3D thin-film device. (b) PXRD patterns of as-prepared Cu-HHTP 3D thin film, TiO<sub>2</sub>-NWAs/sapphire substrate and simulation of Cu-HHTP. (c) *I*-*V* curve of 20 nm Cu-HHTP 3D thin film and TiO<sub>2</sub> NWA substrate. (d) Thickness-dependent response of Cu-HHTP 3D thin film towards 10 ppm NH<sub>3</sub>. Sensing performance of Cu-HHTP-20 nm 3D thin film: (e) concentration-dependent response-recovery curves, (f) response-concentration log-log plots, (g) response towards 5 ppb NH<sub>3</sub>, (h) comparison of response (1 ppm), LOD (ppm) and response time (min) of Cu-HHTP powder, 2D thin film and 3D thin film-based RT NH<sub>3</sub> sensors. (i) Response toward NH<sub>3</sub> and interfering gases of 100 ppm.

PXRD patterns (Figure 3b) verified that 3D thin films on TiO<sub>2</sub>-NWAs are well-crystallized Cu-HHTP. To further demonstrate the continuity of Cu-HHTP thin film on TiO<sub>2</sub> NWAs, the resistance of 3D thin film was measured with a pair of parallel electrodes attached to both edges of Cu-HHTP-20 nm where there are no TiO<sub>2</sub> nanowires (Figure 3a and S9). As shown in Figure 3c, Cu-HHTP 3D thin film exhibited 10 times lower resistance than pristine TiO<sub>2</sub>-NWAs substrate, indicating Cu-HHTP-20 nm was the main conductive path.

Cu-HHTP and its isostructural MOFs are known as candidates for room-temperature gas sensing materials.<sup>[9,25,30,31]</sup> Specifically, Cu-HHTP shows a highly selective response to NH<sub>3</sub>. Preparing Cu-HHTP into 2D thin film has been reported to significantly enhance gas sensing performances. Herein, to demonstrate the strong advantages of MOF 3D thin film, Cu-HHTP 3D thin film was studied as a chemiresistive gas sensing material. The performance of the Cu-HHTP-*x* nm (*x* = 0, 6, 12, 20, 36) 3D thin films were evaluated. Pristine TiO<sub>2</sub>-NWAs substrate showed negligible sensing response to NH<sub>3</sub> at room temperature (Figure S10). Comparatively, significant increments in resistance appeared when exposing Cu-HHTP-*x* nm to NH<sub>3</sub> (Figure 3d,e and S11). Similar to Cu-HHTP 2D thin film, thickness-dependent sensitivity was observed in Cu-HHTP 3D thin film. With increasing thickness, the response of Cu-HHTP 3D thin film

increased firstly, reaching a maximum at 20 nm (Figure 3d), and then decreased. This behavior could be explained by the trade-off between available active sites and gas diffusion length. The relatively thinner film has fewer active sites inside, while the relatively thicker film has a longer gas diffusion path.

As the concentration of NH<sub>3</sub> increased from 1 to 100 ppm, the response increased from 42 to 161%. The device displayed a coefficient of variation (CV) of only 2.13% over five consecutive cycles, indicating outstanding repeatability (Figure 3e). In Figure 3f, the response-concentration log-log plot of Cu-HHTP-20 nm exhibits good linearity in the range of 1–10 ppm. The theoretical limit of detection (LOD) is calculated to be ≈87 ppt from the fitted linear equation by setting the response to be 10%. Compared with Cu-HHTP powder and 20 nm 2D thin film, Cu-HHTP-20 nm exhibited 16100% and 250% higher response (to 1 ppm NH<sub>3</sub>), 5000 and 1000 times lower LOD

(Figure 3h), which may be ascribed to the better gas enrichment ability of this unique 3D structure. Experimentally, Cu-HHTP-20 nm 3D thin film can detect NH<sub>3</sub> with a concentration down to 5 ppb (Figure 3g). Notably, this is one of the lowest LOD among all the reported room-temperature NH<sub>3</sub> chemiresistive sensing materials (Table S1).

The response and recovery time of Cu-HHTP-20 nm toward 100 ppm NH<sub>3</sub> were estimated to be 35 s and 15 min, respectively (Figure S12). Compared to reported Cu-HHTP powder (*T*<sub>res.</sub> = 240 s) and 20 nm 2D thin film (*T*<sub>res.</sub> = 81.6 s), the response speed of 3D thin film is improved by 600% and 130% (Table S2), respectively. As far as we know, Cu-HHTP-20 nm ranks among the fastest reported room-temperature NH<sub>3</sub> chemiresistive sensing materials (Table S1). Its excellent response speed may result from the enhanced mass and charge transport in the preferred-oriented Cu-HHTP 3D thin films. Meanwhile, Cu-HHTP-20 nm also showed a selectivity of >3 towards interference gases (Figure 3i), indicating its excellent selectivity.

In conclusion, aiming to increase the active surface area and optimize the mass and charge transport in MOF thin films, 3D MOF thin film was successfully prepared in a controllable LBL manner for the first time. The prepared semiconducting Cu-HHTP 3D thin films possess good crystallinity, preferred orientation, as well as precisely controllable thickness in nanoscale. The chemiresistive

sensor based on 3D thin film showed 1000 times optimized LOD, 250% enhanced response (to 1 ppm NH<sub>3</sub>), and 130% improved response speed compared with Cu-HHTP 2D thin film. Notably, Cu-HHTP 3D thin film also exhibited one of the highest sensitivity, lowest LOD and fastest response speed among all the reported chemiresistive NH<sub>3</sub> sensing materials at room temperature. The outstanding sensing performances can be attributed to the efficient mass and charge transport, increased active surface area and highly exposed active sites of the orientedly grown high-quality thin film. This work provides a new method for the precise control of MOF thin film growth on nanostructured substrates, giving rise to MOF 3D thin film and MOF-based heterostructures, which may facilitate MOFs' advanced applications such as electronic devices, catalysis, and energy storage devices.

### Acknowledgements

This work was supported by the NSF of China (21822109, 21975254, 21905280, 91961115), the Strategic Priority Research Program of CAS (XDB20000000), International Partnership Program of CAS (121835KYSB201800), and Youth Innovation Promotion Association CAS. Fujian Science & Technology Innovation Laboratory for Optoelectronic Information of China (2021ZR101).

### Conflict of Interest

The authors declare no conflict of interest.

**Keywords:** electrical devices · gas sensors · metal-organic frameworks · semiconductor · thin films

- [1] H. C. Zhou, J. R. Long, O. M. Yaghi, *Chem. Rev.* **2012**, *112*, 673–674.
- [2] S. Kitagawa, R. Kitaura, S. Noro, *Angew. Chem. Int. Ed.* **2004**, *43*, 2334–2375; *Angew. Chem.* **2004**, *116*, 2388–2430.
- [3] V. Stavila, A. A. Talin, M. D. Allendorf, *Chem. Soc. Rev.* **2014**, *43*, 5994–6010.
- [4] C. Dey, T. Kundu, B. P. Biswal, A. Mallick, R. Banerjee, *Acta Crystallogr. Sect. B* **2014**, *70*, 3–10.
- [5] H. Furukawa, K. E. Cordova, M. O'Keeffe, O. M. Yaghi, *Science* **2013**, *341*, 1230444.
- [6] R. Banerjee, H. Furukawa, D. Britt, C. Knobler, M. O'Keeffe, O. M. Yaghi, *J. Am. Chem. Soc.* **2009**, *131*, 3875–3877.
- [7] I. Stassen, N. Burtch, A. Talin, P. Falcaro, M. Allendorf, R. Ameloot, *Chem. Soc. Rev.* **2017**, *46*, 3185–3241.
- [8] N. Wang, Q. Sun, J. Yu, *Adv. Mater.* **2019**, *31*, e1803966.
- [9] M. G. Campbell, S. F. Liu, T. M. Swager, M. Dinca, *J. Am. Chem. Soc.* **2015**, *137*, 13780–13783.
- [10] M. E. DMello, N. G. Sundaram, A. Singh, A. K. Singh, S. B. Kalidindi, *Chem. Commun.* **2019**, *55*, 349–352.
- [11] X. Ma, Y. Chai, P. Li, B. Wang, *Acc. Chem. Res.* **2019**, *52*, 1461–1470.
- [12] A. Schneemann, V. Bon, I. Schwedler, I. Senkovska, S. Kaskel, R. A. Fischer, *Chem. Soc. Rev.* **2014**, *43*, 6062–6096.
- [13] H. W. O. Shekha, S. Kowarik, F. Schreiber, M. Paulus, M. Tolan, C. Sternemann, F. Evers, D. Zacher, R. A. Fischer, C. Wöll, *J. Am. Chem. Soc.* **2007**, *129*, 15118–15119.
- [14] Y. Liu, Y. Wei, M. Liu, Y. Bai, X. Wang, S. Shang, J. Chen, Y. Liu, *Angew. Chem. Int. Ed.* **2021**, *60*, 2887–2891; *Angew. Chem.* **2021**, *133*, 2923–2927.
- [15] I. Hod, W. Bury, D. M. Karlin, P. Deria, C. W. Kung, M. J. Katz, M. So, B. Klahr, D. Jin, Y. W. Chung, T. W. Odom, O. K. Farha, J. T. Hupp, *Adv. Mater.* **2014**, *26*, 6295–6300.
- [16] I. Stassen, M. Styles, G. Greci, H. V. Gorp, W. Vanderlinden, S. D. Feyter, P. Falcaro, D. D. Vos, P. Vereecken, R. Ameloot, *Nat. Mater.* **2016**, *15*, 304–310.
- [17] E. Virmani, J. M. Rotter, A. Mahringer, T. von Zons, A. Godt, T. Bein, S. Wuttke, D. D. Medina, *J. Am. Chem. Soc.* **2018**, *140*, 4812–4819.
- [18] R. Makiura, S. Motoyama, Y. Umemura, H. Yamanaka, O. Sakata, H. Kitagawa, *Nat. Mater.* **2010**, *9*, 565–571.
- [19] R. Dong, T. Zhang, X. Feng, *Chem. Rev.* **2018**, *118*, 6189–6235.
- [20] V. Rubio-Giménez, M. Galbiati, J. Castells-Gil, N. Almora-Barrios, J. Navarro-Sanchez, G. Escorcia-Ariza, M. Mattera, T. Arnold, J. Rawle, S. Tatay, E. Coronado, C. Marti-Gastaldo, *Adv. Mater.* **2018**, *30*, 1704291.
- [21] S. Sakaida, K. Otsubo, O. Sakata, C. Song, A. Fujiwara, M. Takata, H. Kitagawa, *Nat. Chem.* **2016**, *8*, 377–383.
- [22] K. Otsubo, T. Haraguchi, O. Sakata, A. Fujiwara, H. Kitagawa, *J. Am. Chem. Soc.* **2012**, *134*, 9605–9608.
- [23] T. Haraguchi, K. Otsubo, O. Sakata, A. Fujiwara, H. Kitagawa, *J. Am. Chem. Soc.* **2016**, *138*, 16787–16793.
- [24] J. Liu, C. Woll, *Chem. Soc. Rev.* **2017**, *46*, 5730–5770.
- [25] M. S. Yao, X. J. Lv, Z. H. Fu, W. H. Li, W. H. Deng, G. D. Wu, G. Xu, *Angew. Chem. Int. Ed.* **2017**, *56*, 16510–16514; *Angew. Chem.* **2017**, *129*, 16737–16741.
- [26] W.-T. Koo, J.-S. Jang, I.-D. Kim, *Chem* **2019**, *5*, 1938–1963.
- [27] M. S. Yao, W. X. Tang, G. E. Wang, B. Nath, G. Xu, *Adv. Mater.* **2016**, *28*, 5229–5234.
- [28] G. Cai, W. Zhang, L. Jiao, S.-H. Yu, H.-L. Jiang, *Chem* **2017**, *2*, 791–802.
- [29] C. Huang, Z. Guo, X. Zheng, X. Chen, Z. Xue, S. Zhang, X. Li, B. Guan, X. Li, G. Hu, T. Wang, *J. Am. Chem. Soc.* **2020**, *142*, 9408–9414.
- [30] M. G. Campbell, D. Sheberla, S. F. Liu, T. M. Swager, M. Dinca, *Angew. Chem. Int. Ed.* **2015**, *54*, 4349–4352; *Angew. Chem.* **2015**, *127*, 4423–4426.
- [31] M. K. Smith, K. A. Mirica, *J. Am. Chem. Soc.* **2017**, *139*, 16759–16767.

Manuscript received: August 25, 2021

Revised manuscript received: September 23, 2021

Accepted manuscript online: October 11, 2021

Version of record online: November 3, 2021